TECHNISCHE UNIVERSITÄT MÜNCHEN

Bachelor's Thesis in Physics

Blazar Stacking - Sensitivity Analysis for IceCube Neutrino Observatory

Patrick Schaile

15th March 2022

Supervisor: Prof. Dr. Elisa Resconi

Abstract

In modern physics research it is not only of interest to resolve more and more tinier structures and therefore fundamental processes and the underlying physics but one also wants to understand the evolution of the universe and what it is actually made of. In fact astroparticle physics creates a link between those two paths and connects fundamental particles with the prevailing processes in the universe. One great messenger of needed information about astronomical objects and the physics behind is found in neutrinos. To detect these neutrinos the IceCube Neutrino Observatory may be used. The aim of this thesis was to do a sensitivity study for the stacking analysis in IceCube which tries to observe a clustering of neutrinos coming from blazars. It was to set a limit for the minimum neutrino flux, which has to be emitted by a list of considered blazars, so that IceCube would be able to actually observe it. The list of blazars was basically provided by the 4LAC-DR2 catalog [1, 2]. The results of the work lead to necessary constraints for the differential flux of neutrinos coming from these blazars, to be at least

$$\frac{d\Phi}{dE} = 3.43 \cdot 10^{-15} (\mathrm{GeVcm^2 s})^{-1} \left(\frac{E}{E_0}\right)^{-2} \tag{1}$$

for the case of sensitivity and

$$\frac{d\Phi}{dE} = 5.05 \cdot 10^{-15} (\mathrm{GeVcm^2 s})^{-1} \left(\frac{E}{E_0}\right)^{-2} \tag{2}$$

for the case of discovery potential, so that it could be observed with statistical significance. The energy is normalized by $E_0 = 1$ TeV.

Contents

Abstract **i**

1 Introduction **2**

2 Neutrino Physics **5**
2.1 Historic overview 5
2.2 Neutrino Properties 6
2.3 Neutrino Interactions 8
2.4 Atmospheric Neutrinos 10
2.5 Astrophysical Neutrinos 11

3 IceCube Neutrino Observatory **15**
3.1 Detection Principle 15
3.2 Event Topologies 16
3.2.1 Cascade-like Events 16
3.2.2 Track-like Events 17
3.2.3 Double Bang Events 18

4 Point Source Search **21**
4.1 Unbinned Maximum Likelihood Method 21
4.2 Sensitivity and Discovery Potential 24

5 Stacking Analysis on the 4LAC-DR2 catalog **27**
5.1 Concept of the Stacking Analysis 27
5.2 Stacking of Blazars in the 4LAC-DR2 Catalog 28
5.3 Performance of the 4LAC Stacking Analysis 31

6 Conclusion and Outlook **41**

7 Appendix **44**

List of Figures **47**

List of Tables **49**

Bibliography **50**

1 Introduction

The main advantage of using neutrinos as astronomical messengers compared to others like charged particles or photons is that they effectively only underlie the weak force and their cross section is very suppressed in any case. That is, neutrinos are very poorly affected along their way to Earth and therefore point back to their origin. The IceCube Neutrino Observatory, the largest currently operating neutrino telescope which was built at the geographic South Pole and uses the antarctic ice as natural detection material, in general detects events for which it gives information mainly about the energy and arrival direction of the neutrinos causing them. Gathering data from May 2010 to May 2012 IceCube discovered a diffuse astrophysical flux of neutrinos over the conventional atmospheric background it has been observing. Over this time the 28 detected events located in an energy range of $30-1200$ TeV exceeded the expectation of $10.6^{+5.0}_{-3.6}$ based on the assumption of only atmospheric background events. Due to this high energy range and as the events could be modelled by a harder energy spectrum compared to the atmospheric one, the assumption of astrophysical neutrinos reaching IceCube could be justified [3]. Since the origin of this diffuse flux of astrophysical neutrinos could not be identified, this became the next big challenge.
Later on the 22nd of September in 2017 a coincidence of a high energy neutrino event in IceCube and a gamma-ray flare emitted by the blazar TXS $0506+056$ [1] could be found. The neutrino event which was estimated to be around 290 TeV could be associated to the gamma-ray flare on a 3σ spatial and temporal coincidence [4].
Further studies based on IceCube data from September 2014 to March 2015, showed statistical significance on the level of 3.5σ confidence, that TXS $0506+056$ actually portrays a source for high energy neutrinos independent of the single high energy event observed in 2017 [5]. This gives good reason for testing blazars as possible sources of astrophysical neutrinos.
Blazars essentially build a subclass of active galactic nuclei (AGN) which describes a compact region in the middle of a galaxy having a supermassive black hole in its center and a relativistic jet of radiation, including electromagnetic rays as well as massive particles, aligned to the direction to Earth [5]. AGN in general show characteristics in their emission of not being of common stellar origin, such as their high degree in luminosity or the spectral energy distribution. The leading model roughly describing

[1] The gamma-ray flare was detected by the Fermi-LAT

blazars uses collision of matter at the center gained through the accretion disk around the black hole, leading to electromagnetic shock waves and an acceleration of charged particles along the field. In consequence of interactions of the charged primary particles, different particles may be produced, such as high energetic neutrinos [5]. Minding this, blazars are excellent candidates for high energy neutrino sources. Within the work of this thesis I perform a sensitivity study for IceCube, focusing on the statistical significance of a neutrino flux coming from blazars listed in the 4LAC-DR2 catalog. This is done by means of the likelihood-ratio hypothesis test, performed within the stacking analysis in order to evaluate the overall contribution of all the analysed objects to the diffuse astrophysical neutrino flux.

The thesis starts by giving a general overview of the physics of neutrinos, including basic properties, interactions and a categorization of atmospheric and astrophysical neutrinos. The second chapter is about the IceCube Neutrino Observatory, primarily regarding the detection principle and the event topologies. This is followed by a short part explaining the concept of the point source search, mainly defining the hypothesis test and the relevant quantities as well as describing the used unbinned maximum likelihood approach. In chapter 5, apart from giving a description of the stacking analysis, which is based on the point source search, we take a closer look on the 4LAC-DR2 catalog and finally the results of the sensitivity study are discussed. In the end a short conclusion and an outlook of further improvement of the stacking analysis, to possibly become more sensitive, is given.

2 Neutrino Physics

2.1 Historic overview

The neutrino as a particle was first postulated by Wolfgang Pauli in 1930 to consistently solve the energy and momentum conservation for the observed β-decay of the neutron [6]. Back then only a proton and an electron were detected as outgoing particles, while a continuous distribution of momentum and energy for the electron had been observed. For a theoretic two-body decay however the energy and momentum states of the outgoing particles would be constrained to fixed values. Especially assuming that one of the outgoing particles carries almost the whole mass (proton), the lighter particle (electron) then should carry the rest of the momentum to guarantee the overall conservation of such a quantity. However there was a lack of energy observed. Thus the β-decay of the neutron has to be a three-body process

$$n \to p + e^- + \overline{\nu}_e \tag{2.1}$$

in which the postulated neutrino is an uncharged light particle which carries spin $\frac{1}{2}$ to also be consistent with the conservation of angular momentum. In 1956 the first electron anti-neutrino was directly detected by Clyde L. Cowan and Frederick Reines, using the idea of the inverse β-decay

$$p + \overline{\nu}_e \to n + e^+ \tag{2.2}$$

where a specific coincidence of gamma-rays produced by the outgoing neutron being captured by a nucleus and the two characteristic photons coming from annihilation of the outgoing positron and an external electron could be measured [7].

2.2 Neutrino Properties

The neutrino builds a subclass of the Standard Model of particle physics. As the name which was coined by Enrico Fermi might already spoil, it is an electrically uncharged lepton (spin $\frac{1}{2}$) with very low mass, interacting only via negligable gravitational and mostly weak force. As leptons, neutrinos can be divided into three different generations:

$$\begin{pmatrix} \nu_e \\ e^- \end{pmatrix} \begin{pmatrix} \nu_\mu \\ \mu^- \end{pmatrix} \begin{pmatrix} \nu_\tau \\ \tau^- \end{pmatrix}$$

each containing a charged lepton and the corresponding neutrino as well as their respective anti-particles.
One big and still open question about the properties of neutrinos is about their masses. Although the Standard Model predicts massless neutrinos, there is crucial evidence that there are at least two neutrino states with finite mass. The central observation [1] is the phenomenon of ν-oscillations [9]. This means that a neutrino being produced in an eigenstate of the weak interaction ($\nu_{e,\mu,\tau}$) can actually change its flavor while travelling as a free particle. Therefore the neutrino can be detected in a flavor state different from the original one expected from the production process. Thus the three flavor states can be represented by a linear combination of the three mass-/energy-eigenstates ($\nu_{1,2,3}$) which are themselves preserved in time:

$$\begin{pmatrix} |\nu_e\rangle \\ |\nu_\mu\rangle \\ |\nu_\tau\rangle \end{pmatrix} = \begin{pmatrix} U_{e1} & U_{e2} & U_{e3} \\ U_{\mu 1} & U_{\mu 2} & U_{\mu 3} \\ U_{\tau 1} & U_{\tau 2} & U_{\tau 3} \end{pmatrix} \cdot \begin{pmatrix} |\nu_1\rangle \\ |\nu_2\rangle \\ |\nu_3\rangle \end{pmatrix}$$

The describing matrix U is the so called PMNS matrix, short for
Pontecorvo–Maki–Nakagawa–Sakata.
It is an unitary transformation, so that $U^\dagger = U^{-1}$ holds. The boundary conditions on U (unitarity, $detU = 1$, etc.) lead to four parameters, three mixing angles θ_{ij} $(i, j \in 1, 2, 3)$ and one complex phase δ, which determine its entries [10, 11].

[1] In super-kamiokand the K2K-experiment observed the disappearance of ν_μ within a neutrino-beam due to oscillation [8]

A more concrete representation of the PMNS-matrix [2] is then given by:

$$\begin{pmatrix} U_{e1} & U_{e2} & U_{e3} \\ U_{\mu1} & U_{\mu2} & U_{\mu3} \\ U_{\tau1} & U_{\tau2} & U_{\tau3} \end{pmatrix} = \begin{pmatrix} c_{12}c_{13} & s_{12}c_{13} & s_{13}e^{-i\delta} \\ -s_{12}c_{23} - c_{12}s_{23}s_{13}e^{i\delta} & c_{12}c_{23} - s_{12}s_{23}s_{13}e^{i\delta} & s_{23}c_{13} \\ s_{12}s_{23} - c_{12}c_{23}s_{13}e^{i\delta} & -c_{12}s_{23} - s_{12}c_{23}s_{13}e^{i\delta} & c_{23}c_{13} \end{pmatrix}$$

with $s_{ij} = \sin(\theta_{ij})$ and $c_{ij} = \cos(\theta_{ij})$ [12].
Since the mass-eigenstates j fulfill the Dirac equation [3], as they are fermions, the propagation of a neutrino produced in a certain flavor α may be expressed as:

$$|\nu_\alpha(t)\rangle = \sum_j e^{-ip_j\cdot x}\, U_{\alpha j}\, |\nu_j\rangle \tag{2.3}$$

where p_j is the 4-momentum of the $|\nu_j\rangle$ state and $p_j \cdot x$ the scalar-product in the sense of the Minkowski-metric.
Thus the probability to find the neutrino in a flavor state β is simply given by the projection:

$$\langle \nu_\beta | \nu_\alpha(t) \rangle \tag{2.4}$$

Assuming that the neutrino travels at the speed of light, the dependence of the projection on the momenta reduces to the mass differences $\Delta m^2_{ij} = m_i^2 - m_j^2$ and the distance L to the production origin.
With already determined mixing angles θ_{ij} from other experiments, like the Daya-Bay-experiment, the mass differences Δm^2_{ij} may be established [12].
Deputies for experiments of using these oscillations to determine the mass differences are MINOS or KamLand [13, 14].
Furthermore the KATRIN-experiment sets an absolute upper limit for the mass of the electron anti-neutrino [4]. It tries to measure the production rate of electrons at their maximum energy in the β-decay which is very sensitive to the neutrino mass, since the maximum energy carried by an electron is reduced by the mass of the neutrino here [15].

[2] The PMNS matrix is only realized in this form if the neutrino is no Majorana particle. Otherwise an additional matrix would have to be multiplied to the right respecting this. In the here assumed case that neutrinos are Dirac particles this matrix reduces to the identity.
[3] This holds under the assumption that neutrinos are Dirac fermions.
[4] Mind that the electron anti-neutrino is still a superposition of the actual mass-eigenstates as stated before.

2.3 Neutrino Interactions

As mentioned, the neutrinos are very light particles and therefore mostly only interact via weak force, since they are uncharged leptons. In theory fermions are described by four-dimensional spinors Ψ which can be separated into two two-dimensional spinors [5], that is $\Psi = \begin{pmatrix} \chi_L \\ \chi_R \end{pmatrix}$. Since the two transform separately under Lorentz-boosts in the Weyl-basis [6], they actually can underlie interaction processes independently and in different ways. This is indeed realized in the weak interaction, where the $W^{\pm}$-bosons [7] in charged currents (CC) only couple to the χ_L-part of particles and only to the χ_R-part of antiparticles. Furthermore for massless particles the helicity (projection of spin onto momentum) is the same as the chirality so in this case there are only produced left-handed particles and right-handed anti-particles. Due to their very low mass this is in fact what is practically observed for neutrinos. As of now there are only left-handed ν and only right-handed $\overline{\nu}$ observed. Independent on if there will be evidence for right-handed neutrinos in the future, it should be mentioned that there has to be physics beyond the Standard Model as it anyhow only predicts massless neutrinos.
Back to the possible interactions, in the neutral current (NC) where an uncharged Z^0-boson is exchanged the involved neutrino stays the same and a hadronic cascade can be produced ($\nu_l + N \rightarrow \nu_l + N^*$).
On the other hand the CC forces the involved neutrino to change into the corresponding lepton of its generation, while electric charge is transmitted ($\nu_l + N \rightarrow l + N^*$) and a hadronic cascade may be produced in the interaction vertex.
Considering a neutrino weakly interacting with a nucleus via CC, for energies below ~0.1 GeV the target nucleus behaves like a point-like particle [16]. For energies above 20 GeV, which is the relevant energy range in the antarctic ice at IceCube, the neutrino scatters deep inelastically on the nucleus so the quark structure is resolved and a hadronic cascade may be produced [16]. The latter process is illustrated in a Feynman-diagramm in 2.1.

[5] $\chi_{L/R}$ means the two dimensional left-/right-chiral spinors respectively.

[6] The Weyl-basis is a basis in which the spinor Ψ might be described just like the Dirac representation. Both can be translated by unitary transformations.

[7] Indeed the Z^0-boson does not show a maximum parity violation and couples to both chirality-parts of the spinor.

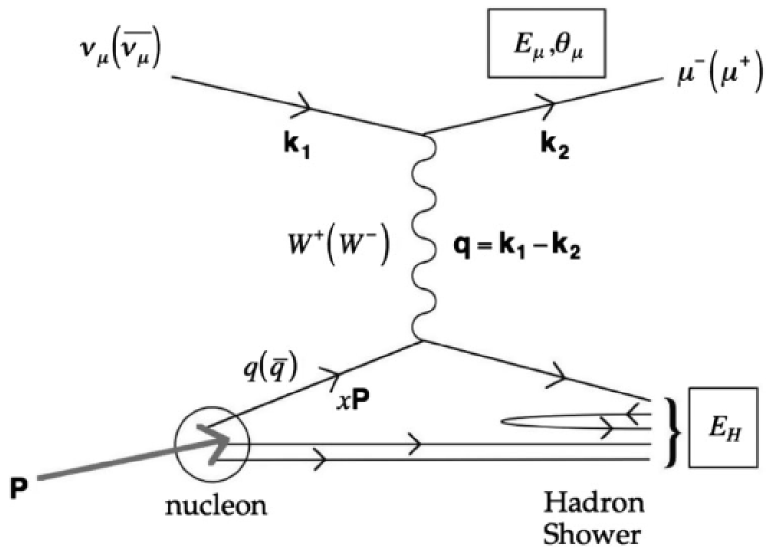

Figure 2.1: Feynman diagram of deep inelastic scattering (DIS) for a muon (anti-) neutrino off a nucleus via the exchange of a $W^{\pm}$-boson (CC) where also a hadronic shower is produced. The outgoing muon can be detected as evidence. At each vertex here the conservation of momentum, charge and the leptonic flavor is respected [16].

.

2.4 Atmospheric Neutrinos

Atmospheric neutrinos describe all neutrinos produced in Earth's atmosphere by other particles interacting with molecules of the air. The primary particles responsible for this are found in the cosmic ray (CR) which are fully ionized nuclei, mainly of Hydrogen, i.e. protons, Helium and only few heavier elements [17]. The measured energy spectrum of cosmic rays is shown in figure 2.2. The differential flux can be modelled by a power law, explicitly $d\Phi/dE \propto E^{-\gamma}$, with $\gamma = 2.7$ up to the 'knee' at about 10^6 GeV, where the spectrum hardens to $\gamma = 3.0$ until it comes back to $\gamma = 2.7$ at the 'ankle' 10^9 GeV. Above about 10^{10} GeV the CR is strongly suppressed, due to interactions with the cosmic microwave background. Consequently the universe would become opaque for the primary particles at high energies [17].

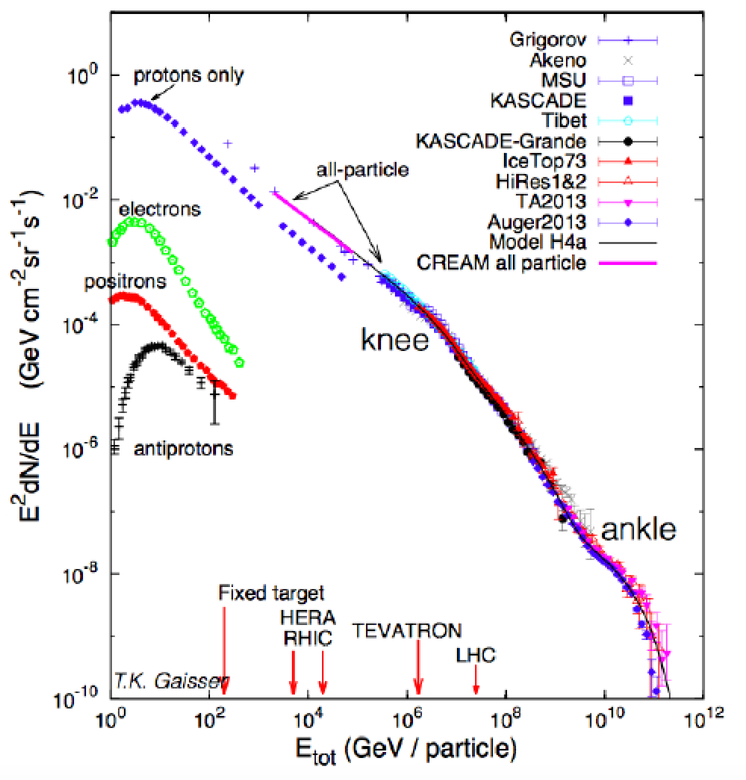

Figure 2.2: The figure shows the differential flux of the cosmic ray in an energy range form 1 - 10^{12} GeV. It turns out that it can be described by power law dependencies, $d\Phi/dE \propto E^{-\gamma_i}$, for several sub-regions i of the considered energy spectrum. [18]

Charged mesons, like pions and kaons and therefore muons are produced as secondary particles when the primary CR (e.g. protons) interacts with ambient matter in the upper atmosphere in so-called hadron-hadron-collisions. When the secondary mesons decay they produce, among other particles, neutrinos. The dominant decay processes are:

$$\pi^{\pm} \rightarrow \mu^{\pm} + \nu_{\mu}(\overline{\nu}_{\mu}) \tag{2.5}$$

$$K^{\pm} \rightarrow \mu^{\pm} + \nu_{\mu}(\overline{\nu}_{\mu}) \tag{2.6}$$

$$K_L^0 \rightarrow \mu^{\pm} + e^{\mp} + \nu_e(\overline{\nu}_e) \tag{2.7}$$

Since the flux of primary particles can be described by $d\Phi/dE \propto E^{-2.7}$ and a relevant amount of the secondary pions and Kaons depose a fraction of their energy in interactions with matter before decaying, the differential atmospheric flux of neutrinos can be modelled by a more shallow $E^{-3.7}$ dependence. The flavor ratio for atmospheric neutrinos turns out to be (2 : 1 : 0) $(\nu_{\mu}, \nu_e, \nu_{\tau})$ below 3 GeV and (20 : 1 : 0) at about 1 TeV [19].

2.5 Astrophysical Neutrinos

The interesting part in neutrino search is about astrophysical neutrinos. Since these particles are barely affected by interactions with matter and radiation while travelling through space, they are not as deviated as charged particles and do not lose as much as energy as photons do. Thus they are great astronomical messengers and can give information about the production processes inside the source. In general, photonuclear-

$$p\gamma \rightarrow \Delta^{+} \rightarrow \begin{cases} p\pi^0 \\ n\pi^{+} \end{cases} \tag{2.8}$$

or proton-proton-collisions

$$pp \rightarrow \begin{cases} pp\pi^0 \\ pn\pi^{+} \end{cases} \tag{2.9}$$

deliver important neutrino production processes by generating secondary decaying mesons which then behave similarly to the atmospheric produced ones, which is given by 2.5 - 2.7 [20]. The model of the First order Fermi acceleration which delivers explanation for the generation of particle jets in blazars, describes primary charged particles (like protons) being gathered by the AGN and accelerated through electromagnetic shock fronts [21]. The particles may then underly the interaction processes from above, producing astrophysical neutrinos. Figure 2.3 gives a general illustration of the situation about neutrino fluxes, including the atmospheric flux as well as astrophysical neutrinos.

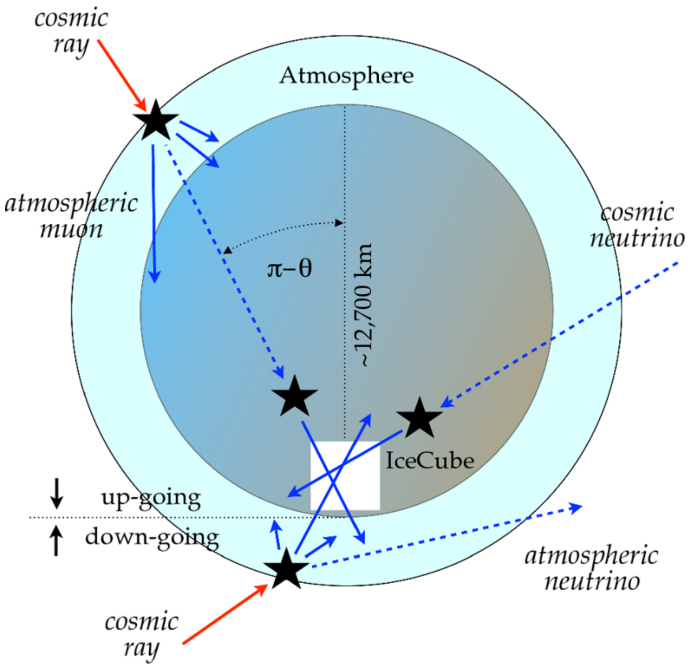

Figure 2.3: The figure gives an illustration of the general situation for IceCube detecting atmospheric and astrophysical neutrino events [22]

Further the measurements of the different power law dependencies of atmospheric and astrophysical neutrino fluxes are shown in the following figure 2.4

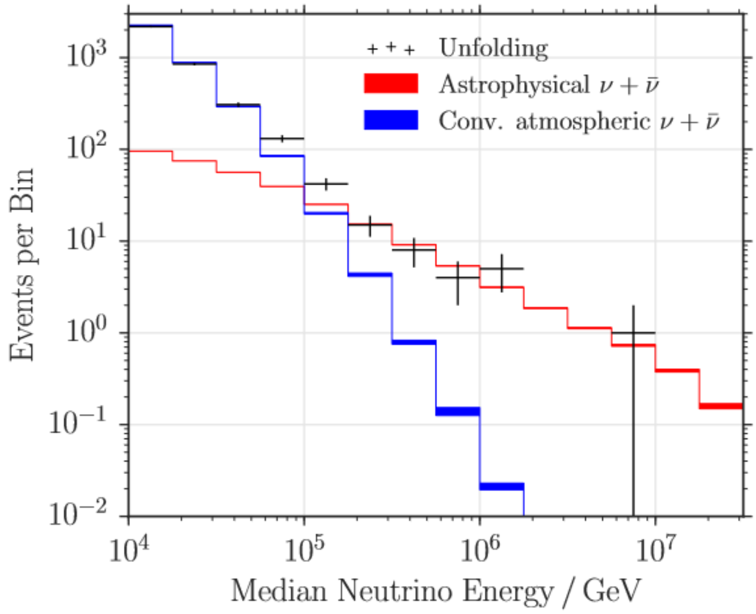

Figure 2.4: The plot shows the dependence of the neutrino fluxes observed by IceCube on the neutrino energy, i.e. the conventional atmospheric background and the diffuse astrophysical component. The y-axis which shows the counting for events in one bin which is proportional to the differential flux and is therefore considered equivalent in this context. The blue curve shows the behaviour of atmospheric neutrinos whereas the red one shows the behaviour of the diffuse astrophysical neutrino flux. The two curves are obtained by best-fit parameters which model the differential fluxes respectively The black crosses are experimental data for the observed total flux.[23]

3 IceCube Neutrino Observatory

The IceCube Neutrino Observatory is a large volume neutrino telescope placed at the South Pole, as a part of the Amundsen-Scott South Pole Station. In a depth of around 1500m-2500m, it uses one cubic kilometer of the antarctic ice as detection material. The incoming astrophysical or atmospheric neutrinos interact with the nuclei of the ice as described in 2.3. To measure secondary particles, produced in these interactions, like electrons, muons or tauons, IceCube uses 86 strings, arranged in a hexagonal structure underground each consisting of 60 digital optical modules (DOMs), containing photomultiplier tubes (PMTs) to convert Cherenkov light produced by these secondary charged particles into an electrical signal. The detector also includes the inner 'DeepCore', showing higher density of strings and the 'IceTop' which lies on the surface and consists of 324 DOMs in 81 stations [24].
An illustration of the detector is shown in figure 3.3.

3.1 Detection Principle

The detection principle in IceCube is based on incoming neutrinos weakly interacting with the nuclei of the antarctic ice in either NC- or CC-processes. DIS in CC-process causes a hadronic shower and a charged lepton of the same flavor as the primary neutrino. The charged lepton as a relativistic particle produced by high energy neutrino interaction inside the ice may cause light emission due to the Cherenkov-effect. The Cherenkov-effect describes a cone of light emission along the axis of a charged particle moving through a dielectric medium (here ice) faster than the speed of light $c_n = c/n$ (n is the refractive index) in this medium.
As the illustration 3.1 states, the relativistic charged particle causes electromagnetic emission of the polarized medium, which can then be seen as an in-phase superposition of the electromagnetic emissions, building a 'plane' electromagnetic wave travelling on a cone through the dielectric.

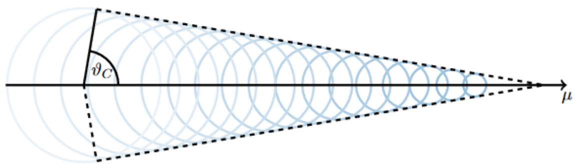

Figure 3.1: Illustration of the Cherenkov-effect. The figure shows the emitted cone of Cherenkov light, including the opening angle for the example of a muon-track [25].

The opening angle θ_C of the cone is given by $\cos(\theta_C) = (\beta n)^{-1}$. The light yield describing the number of Cherenkov photons N can be determined by the Frank-Tamm-equation [17]: $d^2N/dxd\lambda = 2\pi\alpha/\lambda^2 \left(1 - \frac{1}{\beta^2 n^2(\lambda)}\right)$
where x is the coordinate along the track-axis, λ the wavelength of the emitted light and $\alpha = \frac{e^2}{4\pi\epsilon_0 \hbar c}$ the fine-structure constant. The $1/\lambda^2$-dependence shows why the Cherenkov light appears mostly blue, due to its shorter wavelength.

3.2 Event Topologies

In dependence on the flavor of the neutrino and the underlying interaction process, NC or CC, the events in IceCube may appear in different manners. An illustrative overview of the several event topolgies is given in figure 3.2.

3.2.1 Cascade-like Events

Cascades happen when all or most of the neutrino's energy is deposited in a small region around the interaction vertex and result in a nearly spherical shaped event. Cascades are in general more difficult to reconstruct than track-like events, but carry the advantage that all or at least most of the neutrino's energy is deposited inside the detector, which can then be measured [25]. Cascades appear either in NC-processes for all neutrino flavors or also CC-processes for electron neutrinos. The former process produces an electron and a hadronic cascade. The electron may then further interact with the detector material and lose energy by ionization (described by the Bethe-Bloch formula [17]). At some critical energy E_c, which is around $E_{c,e} \approx 90$ MeV for the glacial ice in IceCube, the electron rather loses its energy by radiation than by ionization [17, 18]. The radiated photons may then result in electron-positron pairs via pair production, in case the energy is sufficiently high ($E_\gamma \geq 2m_e$).
Due to the small maximum travel distance in the ice, e.g. ≈ 6.6 m for electrons at 10

Tev, the cascades are almost spherical symmetric [17, 18, 26].

3.2.2 Track-like Events

Tracks in IceCube are mainly caused by muons, produced in CC-processes either inside the detector volume (starting tracks) or coming from outside (through-going tracks). Due to the higher mass of muons, $m_\mu \approx 200 m_e$, the critical energy where radiation dominates ionization is increased to $E_{c,\mu} \approx 500$ GeV [18, 26].
Using the differential energy loss per distance: $dE_\mu / dx = A + B \cdot E_\mu$
with $A = 2.4 \cdot 10^{-3}\mathrm{GeVg}^{-1}\mathrm{cm}^2$ and $B = 3.2 \cdot 10^{-5}\mathrm{g}^{-1}\mathrm{cm}^2$ for energies above the critical $E_{c,\mu}$ for muons and minding their lifetime $\tau_\mu = 2.197 \cdot 10^{-6}$s one gets to a maxmimum travel distance per muon-energy $\approx 4.55\ \mathrm{mGeV}^{-1}$. For instance a muon at around 10 TeV easily exceeds the detector with a maximum travel distance of around 45 km [18, 27]. The energy loss by Cherenkov radiation is negligible compared to the other processes, but the information gained from the effect is of crucial relevance for reconstructing the arrival direction and the energy of the neutrino.
Eventually the interaction of a muon neutrino ν_μ in a CC-process inside IceCube results in a light yield from the hadronic cascade at the interaction vertex and a bright track due to the Cherenkov-effect of the secondary produced muon [18, 27].
Muon tracks provide the best directional reconstruction for neutrino events in IceCube [3]. The relevant limit of the angular resolution for the reconstructed neutrino direction is set by: $\langle \angle(\nu_\mu, \mu) \rangle = \frac{1.5^\circ}{\sqrt{E/\mathrm{TeV}}}$ [18, 27]. This means that the mean angular distance for the reconstructed arrival directions of the muon and the actual neutrino is modulated by the energies of the particles. The resolution gets sharper the higher the energies.

For the work presented in this thesis a sample consisting of about 670 000 up-going muon tracks from the Northern Hemisphere is used, collected over a time span of 9 years from 2011 to 2019. Not least that only a small part ($\mathcal{O}(1000)$) of the tracks were expected to be of cosmic origin, the efficiency of the detector plays a crucial role to actually obtain a sufficiently large data sample of astrophysical event, so it could significantly be seen over the background [28]. IceCube is in fact more sensitive to astrophysical events from the Northern Hemisphere, due to the fact that the Earth might shield an important amount of the large background. That is also why the analysis in this work is restricted to the northern sky. It should be mentioned in this context that IceCube is indeed most sensitive for astrophysical events at the horizon and gets less sensitive up to the North, since the larger travel distances through Earth increase the probabiltiy for a neutrino to interact with the ambient matter and therefore might be shielded off for IceCube at the South Pole.

3.2.3 Double Bang Events

Double bang events refer to events caused by tau neutrinos in IceCube. Due to the high mass of tau leptons, $m_\tau \approx 3500\ m_e$, they are only affected to energy loss through ionization. Moreover due to their very short lifetime, $\tau_\tau = 2.906 \cdot 10^{-13}$ s, after being produced accompanied by a hadronic cascade at the vertex, the tauons cause a track of Cherenkov radiation which is followed by a second hadronic cascade, due to the decaying process [18, 26]. Since tau neutrinos are only produced in prompt decays of heavy mesons with charm contribution which is nearly totally suppressed in atmospheric processes, for an observation which can be associated to a tau neutrino interaction it is almost sure that it is an astrophysical event [18, 29].

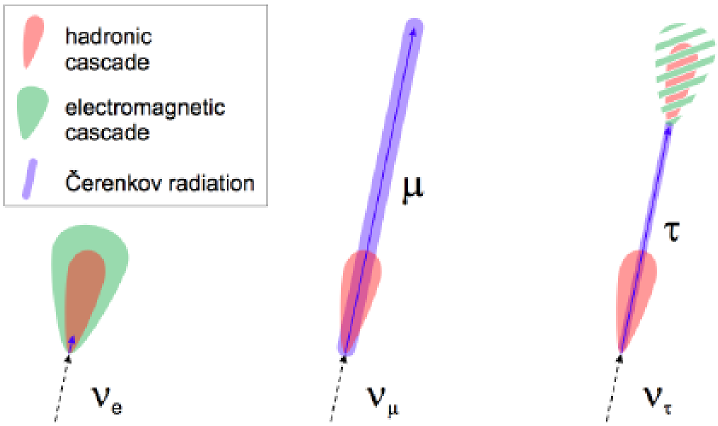

Figure 3.2: This figure is a visual representation of the different event topologies that might appear in IceCube caused by neutrinos of different flavors crossing the detector [30].

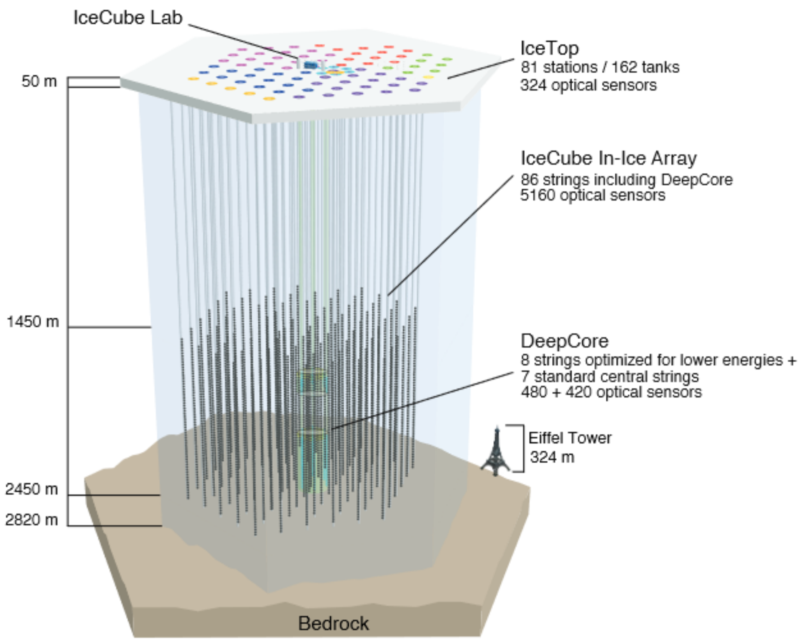

Figure 3.3: Illustration of the detector of IceCube Neutrino Observatory. It consists of the IceCube Lab (laboratory on the ground), IceTop (an surface array on top) and the IceCube in-ice array, placed underground in the antarctic ice [23]. To compare the size of the detector the Eiffel tower is placed next to it to scale.

4 Point Source Search

4.1 Unbinned Maximum Likelihood Method

The general background of the used method is a hypothesis test performed on the reconstructed variables of IceCube's events, namely the muon energy E_i, the muon arrival direction x_i and the uncertainty on the reconstructed direction σ_i. Thus the point source analysis tests the compatibility of a clustering of neutrinos at a specific location in the sky with the background hypothesis. The background here means the conventional atmospheric produced neutrinos and the diffuse astrophysical neutrino flux. The analysis therefore tells whether a certain clustering of neutrinos at a specific point actually would be compatible to the observed background and if there is any excess of astrophysical neutrinos coming from the tested location assuming only background events. A direct way to do this would be a binned method, where the detector is divided into bins of the size of its resolution and one is counting for events exceeding the expectation based on the defined background. But since there would be a loss of information due to the fact of weighting events the same, no matter if they are at the border or the center of a bin, the unbinned maximum likelihood method is used [31]. The performed statistical analysis compares two different hypotheses:

Null Hypothesis H_0**:** The data consists of conventional atmospheric and diffuse astrophysical background

Signal Hypothesis H_1**:** The data consists of both, conventional atmospheric and diffuse astrophysical background, as well as a clustering of N neutrino events at a tested location, showing a power law dependence $\sim E^{-\gamma}$ for the emitted neutrino flux

The central quantity for a statistical test is the test statistic, defined as:

$$\mathcal{TS} = -2\ log \left[\frac{P(H_0|data)}{P(H_1|data)} \right] \tag{4.1}$$

where $P(H_j|data)$ is the likelihood of the hypothesis H_j under the condition of a received data sample. This implies that for larger values of $\mathcal{TS}$ it is more likely that the data is of signal hypothesis origin and is less compatible with the null hypothesis.

Starting from a single point source in the binned case and assuming a poissonian distribution [1] of the detected events k_i around some mean number n_i for the bin i, the likelihood function describing the probabilities above is defined as:

$$\mathcal{L} = \prod_i^{N_{bins}} \frac{n_i^{k_i}}{k_i!} e^{-n_i} = e^{-N} \prod_i^{N_{bins}} \frac{n_i^{k_i}}{k_i!} \quad , \mathrm{N} = \sum_{\mathrm{i}} \mathrm{n_i} \tag{4.2}$$

Setting the number of bins $N_{bins} \to \infty$, i.e. in the unbinned limit ('continuous' detetctor structure), one gets to the discrete case where $k_i = 0, 1$ and the limit of the product sum can be replaced by the number of total events $N (= n_S + n_B)$. n_S stands for the expected number of signal events whereas n_B is the expected number of background events. Staying in the limit of $N_{bins} \to \infty$ one is left with:

$$\mathcal{L} = e^{-N} \prod_i^N (N \cdot p_i \cdot dx) \tag{4.3}$$

where p_i is the probability density function (PDF) to obtain the event i assuming the respective hypothesis H_j to be true. The PDF can be split into signal (S_i) and background (B_i) PDFs independently, i.e.

$$p_i = n_s / N \cdot S_i(x_i, \sigma_i, E_i | x_s, \gamma) + n_B / N \cdot B_i(x_i, E_i) \tag{4.4}$$

Since the null hypothesis is realized by putting $n_s = 0$, thus $\mathcal{L}_{H_0} = \mathcal{L}(n_s = 0)$ and after dropping constant prefactors, the test statistic reduces to:

$$\mathcal{TS} = 2 \sum_i log \left[\frac{n_s}{N} (S_i / B_i - 1) + 1 \right] \tag{4.5}$$

[31]

As the likelihood formalism and later the stacking analysis use positional arguments, they should shortly be explained here. The used parameters containing information about arrival directions of the events or also the position of the point source are characterized by the tuples (α, δ). As they stand for right ascension and declination, they are the coordinate parameters in the used equatorial coordinate system ($J2000$). It is a galactic coordinate system, based on a conventional spherical one. $0°$ in declination indicates the equatorial plane with positive values in the Northern Hemisphere. The right ascension therefore refers to an azimuth angle.

[1] This is a valid assumption since the detection here can be modelled by a counting experiment. For further explanation see 7.

Back to the explicit formalism, the background PDF is uniform in the right ascension and only depends on the declination δ_i of the arrival direction, the uncertainty σ_i and the energy E_i of the measured neutrino. The PDF is therefore given by:

$$B_i(x_i, E_i) = \frac{1}{2\pi} B_i(\delta_i, E_i, \sigma_i) \tag{4.6}$$

The background PDF, including spatial and energy dependencies, can then be achieved numerically through Monte Carlo simulations using models which describe the atmospheric and diffuse astrophysical fluxes. For instance the energy dependent differential flux can respectively be modelled by power laws $\sim E^{-\gamma}$ for the atmospheric $\gamma = 3.7$ and the diffuse astrophysical component $\gamma = 2.28$ [32].
Further the signal PDF can be separated into a spatial and energy dependent part, using the law of conditional probabilities:

$$S_i(x_i, \sigma_i, E_i | x_s, \gamma) = \frac{1}{2\pi\psi_i} \mathrm{S}_i(\psi_i | E_i, \sigma_i, \delta_{src}, \gamma) \cdot \varepsilon_i(E_i | \delta_{src}, \gamma) \tag{4.7}$$

where $\psi_i = ||d_i - d_{src}||$ is the angular distance of the reconstructed arrival direction d_i and the location d_{src} of the tested point source. The prefactor $\frac{1}{2\pi\psi_i}$ expresses the normalization of the PDF [28]. The energy part ε_i contains the dependence on the declination δ_{src} and the neutrino flux,i.e. γ of the source. The latter is based on a power law description

$$\frac{d\Phi}{dEd\Omega} = \Phi_0 \cdot (E/E_0)^{-\gamma} \tag{4.8}$$

of the emitted flux. While $x_{src} = (\alpha_{src}, \delta_{src})$ describes the position of the point source, the parameter $x_i = (d_i, E_i, \sigma_i)$ is the received data set of the IceCube event i. Previous IceCube analyses approximated the spatial term as a Gaussian

$$\mathrm{S}_i(x_i, \sigma_i | x_s) = \frac{1}{\sqrt{2\pi\sigma_i^2}} \exp\left(\frac{||x_i - x_s||^2}{2\pi\sigma_i^2}\right) \tag{4.9}$$

that is independent of the source's spectral index. However the improved and most recent method generates the PDFs 4.6 and 4.7 numerically through Monte Carlo simulations [28]. Finally the obtained $\mathcal{TS}$ value for testing a point source under the condition of a whole data sample x, is a function depending on the likelihood which is maximized with respect to the undetermined parameters n_s (total number of expected signal events) and γ (modelling the power law of the astrophysical flux $\sim E^{-\gamma}$):

$$\mathcal{TS} = -2\ log\left(\frac{\mathcal{L}(n_s = 0|x)}{\sup_{n_s,\gamma} \mathcal{L}(n_s, \gamma|x)}\right) \tag{4.10}$$

[28].
In the present case of multiple point sources this can basically be expanded by summing over all sources, that is carried out more in the 'Stacking Analysis' chapter (5).

4.2 Sensitivity and Discovery Potential

Now to proceed with this and practically conduct the hypothesis test it is to define the p-value p. The p-value is a quantity indicating how extreme a result is under the assumption of validity of the null hypothesis H_0. In the present case a right sided hypothesis test is performed, since the relevant results exceeding the expected outcomes under H_0 are found in large $\mathcal{TS}$ values. Given a PDF $P(\mathcal{TS})$ in the space of the test statistic, the p-value is defined as the probability for values to be larger than some certain threshold $\widetilde{\mathcal{TS}}$ under a valid null hypothesis H_0:

$$p = p\left(\widetilde{\mathcal{TS}}\right) = P\left(\mathcal{TS} \geq \widetilde{\mathcal{TS}}|H_0\right) = 1 - \int_0^{\widetilde{\mathcal{TS}}} P\left(\mathcal{TS}|H_0\right) d\mathcal{TS} \tag{4.11}$$

The smaller the p-value the more extreme is the result assuming the null hypothesis to be true.
Based on this, one defines the sensitivity and discovery potential.
Sensitivity: p-value ≤ 0.5 in 90% of the cases for the obtained $\mathcal{TS}$ values.

Discovery potential: p-value $\leq 3\sigma$ in 50% of the cases for obtained $\mathcal{TS}$ values.
(Here in this case the confidence is set to 3σ, while also the stronger 5σ-convention is commonly often used.)
Minding this, the concept of sensitivity and discovery potential is used to decide on whether to keep or dismiss the null hypothesis. That is, specifically for the discovery potential if 50% of the obtained $\mathcal{TS}$ values show a p-value smaller than 0.00135 the null hypothesis H_0 is disfavoured with respect to the signal hypothesis H_1 [2].
Finally it should be mentioned that even a high statistical evidence that the null hypothesis should be rejected does not assure that the signal hypothesis is correct. One can only conclude on the defined confidence level that the signal hypothesis seems to describe the data better than the null hypothesis. This is quantitatively expressed in the type I and type II errors. The type I error describes the probability α of falsely rejecting the null hypothesis H_0, despite being correct. The type II error addresses the probability β of sticking to the null hypothesis, despite being false and signal hypothesis H_1 being true.

[2] The case for sensitivity is analogous.

All possible outcomes are illustrated in table 4.2.

Decision / Truth	H_0 is true	H_0 is false
accepting H_0	Correct decision $p = 1 - \alpha$	Type II error $p = \beta$
rejecting H_0	Type I error $p = \alpha$	Correct decision $p = 1 - \beta$

Following this scheme for the sensitivity the type I error is $\alpha = 0.5$ and the type II error is $\beta = 0.1$. For discovery potential the type I error is forced to $\alpha \approx 0.00135$ and the type II error is $\beta = 0.5$.

A visualization of the general situation of the hypothesis test is given in figure 4.1 below.

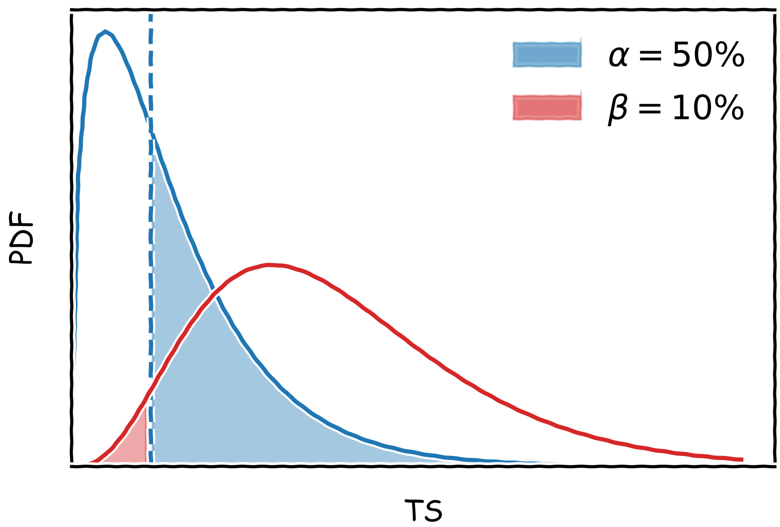

Figure 4.1: This sketch should give an illustration of the overall situation of a hypothesis test. The blue curve represents the $\mathcal{TS}$ PDF obtained under the assumption that the null hypothesis is valid. here in this work this is realized by assuming only background events. The red curve shows the $\mathcal{TS}$ PDF in the case that the defined signal hypothesis corresponds to the truth. The sketch shows the example for sensitivity where for 90% of the cases the $\mathcal{TS}$ values gained under the signal hypothesis are larger than the median of the PDF for a valid null hypothesis. The case of discovery potential is analogous.

5 Stacking Analysis on the 4LAC-DR2 catalog

5.1 Concept of the Stacking Analysis

Based on the same concept as stated in chapter 4.1, the stacking method expands the approach of a single source candidate to a set of M considered possible point sources. Therefore the signal PDF for an event in IceCube used in equation 4.5 is replaced by the weighted sum of signal PDFs over all sources:

$$S_i \rightarrow S_i^{stack} = \sum_{k=1}^{M} W^k \cdot R^k(\delta_k, \gamma) \cdot \mathrm{S}_i^k(x_i, x_{s,k}, E_i) \cdot \varepsilon_i(E_i, \gamma) \tag{5.1}$$

One of the weights applied, namely $R^k(\delta_k, \gamma)$ relates to the efficiency of the detector. The detection efficiency strongly depends on the one hand on the arrival direction of the neutrino and therefore on the Declination δ_k of the source placed at $x_{s,k}$ and on the other hand on the energy of the event, which is modulated by the power law dependence $E^{-\gamma}$ of the neutrino flux emitted by the blazars. In this work the latter is set to $\gamma = 2.0$. Thus relative weights have to be applied for different arrival directions and the energy spectra of the candidates. The numerical values of R^k can be obtained through Monte Carlo simulations [33].
The applied values of W^k respect individual properties of the sources and are independent on the exact position $x_{s,k}$ and the spectral energy parameter γ. The weights W^k leave space for properties such like different $\nu-$emission strengths. Here in this work an equal strength of $\nu-$emission for every of the possible sources was assumed, since we had no significant hint that the considered blazars would have different emission strengths.

Further the weights had to be normalized, i.e. $\sum_{k=1}^{M} W^k R^k = 1$ [33].
The rest of the concept introduced for the case of a single source, like the PDF for the background and the likelihood formalism itself stayed the same.

5.2 Stacking of Blazars in the 4LAC-DR2 Catalog

Due to the spatial and temporal coincidence of a high energy neutrino event observed in IceCube and a detected gamma-ray flare in 2017 which could be associated to the blazar TXS $0506 + 056$ and since analyses of previous IceCube data showed statistical significance that this blazar could be indeed a source for astrophysical high energy neutrinos, further experiments and analyses of testing blazars as point sources for neutrinos appear to be reasonable. However, even after the observation of the diffuse astrophysical flux by IceCube in 2013 which showed statistical evidence for astrophysical neutrinos arriving at IceCube, the expected contribution of a single source is very small for assuming blazars as point sources (see also 1).

Thus point source searches for single considered objects have not been successful in the past. The stacking analysis as an expansion of the single point source search to a set of several point sources is more sensitive and might help out. Based on this idea, this thesis provides a sensitivity study for the stacking analysis performed in the IceCube Neutrino Observatory.

The first step to this was to obtain a list of blazars which should be tested as point sources. A proper list was provided by the 4LAC-DR2 catalog. The 4LAC-DR2 is the second data release of the 4LAC which is the fourth catalog of active galactic nuclei (AGNs) detected by the Fermi Gamma-ray Space Telescope (Fermi-LAT) [1, 2]. It shows the same structure and basic properties but is an update and improvement of the first data release of the 4LAC catalog and is based on data gathered over 10 years. The 4LAC is derived from the 4FGL catalog which lists gamma-ray [1] sources in general and therefore includes the yet observed AGNs. The AGNs included in the 4FGL could be distinguished from other gamma-ray sources by comparing the characteristics of AGNs to the rest of the catalog. The classification of a general gamma-ray source listed in the 4FGL catalog as an AGN was primarily based on its characteristic traits in the optical spectrum. Further properties such as time dependent emissions or the radio loudness were used as ancillary information [1]. The derived 4LAC catalog therefore lists AGN and some of their main properties like the position in ($J2000$) equatorial coordinates or the redshift and the synchrotron peak frequency $\nu_{s,peak}$, if measured respectively. The AGNs in total cover an energy range from 50 MeV - 1 TeV [1, 2].

The 4LAC-DR2 catalog could be accessed in two samples, one listing AGN of high ($|b| > 10°$) and the other one listing AGN of low ($|b| < 10°$) latitude b. The latitude is one of the two parameters of a galactic coordinate system. The galactic coordinate system can be compared to the equatorial one used within this work and can

[1] In the field of astrophysics gamma-rays are conventionally photons which show energies of 100 kev and above.

basically be translated by rotation. Furthermore the latitude could be compared to the declination in equatorial coordinates, where $b = 0°$ descibes the galactic plane. The galactic plane is also the reason why the low latitude AGNs had to be treated differently and were stored separately. Since the galactic plane causes extinction of the emission from AGNs located near $b = 0°$, the flux detection limit for their observation is increased and therefore they had to be treated separately . In fact this effect can be observed in the distribution of the detected sources, since there is a slightly decreased number of sources listed near $b = 0°$. In figure 5.5 which is shown in the context of the Performance of the stacking analysis the effect can be seen, too.

Blazars make up 98% of the AGNs listed in the 4LAC-DR2. A key property of blazars to distinguish them from the rest of the AGNs, for example Steep Spectrum Radio Quasars (SSRQs), is the variability of their emission in time. In total 75% of the classifications here for blazars are based on the characteristics of the spectral energy density and an associated synchrotron peak frequency $\nu_{s,peak}$ [1]. The distribution of the synchrotron peak frequencies for the blazars which should be tested in the sense of this work is given by figure 5.2. Further the blazars can be divided into three subclasses, namely Flat-Spectrum Radio Quasars (FSRQs), BL Lacertae objects (BL Lacs) and Blazars Candidates of Uncertain (BCUs) type. FSRQs show strong emission lines in the optical spectrum as well as a softer spectrum and a stronger variability in the gamma-ray band. BL Lacs however have weak to no lines in the optical emission and show a harder spectrum in the gamma-ray band. The last classification of BCUs means all blazar candidates of yet unknown type [1]. The blazars were already marked and classified in the 4LAC catalog and therefore could be easily accessed for the purpose of this work. From all blazars listed in the catalog only 1916 which are located in the Northern Hemisphere (declination $\delta \in [-3, 81]°$) were taken into further consideration. This belongs to the mentioned fact that the work is based on only up-going muon-tracks detected in IceCube over a time span of 9 years which respects the higher sensitivity of IceCube for astrophysical neutrino events from the Northern Hemisphere and therefore improves the stacking analysis (see also 3.2.2).
Figure 5.1 delivers an artistic illustration of a blazar emitting radiation and a flux of neutrinos to the direction of Earth.

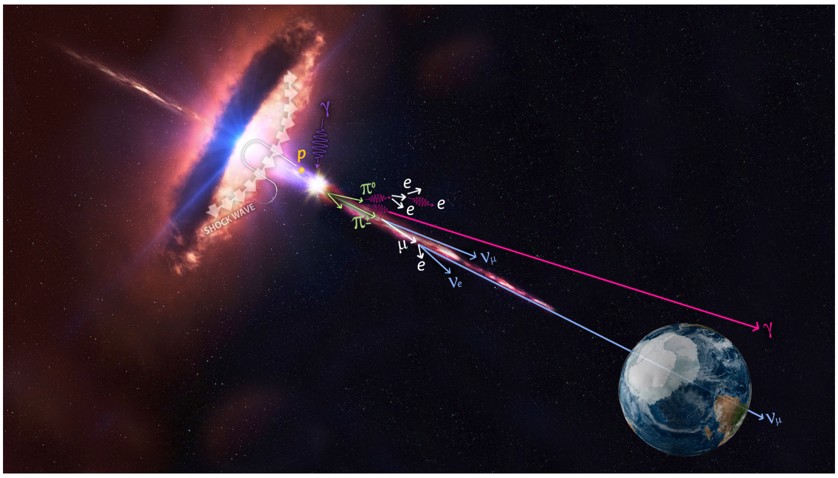

Figure 5.1: Artistic illustration of the general situation assuming that blazars are actual sources of astrophysical neutrinos [34].

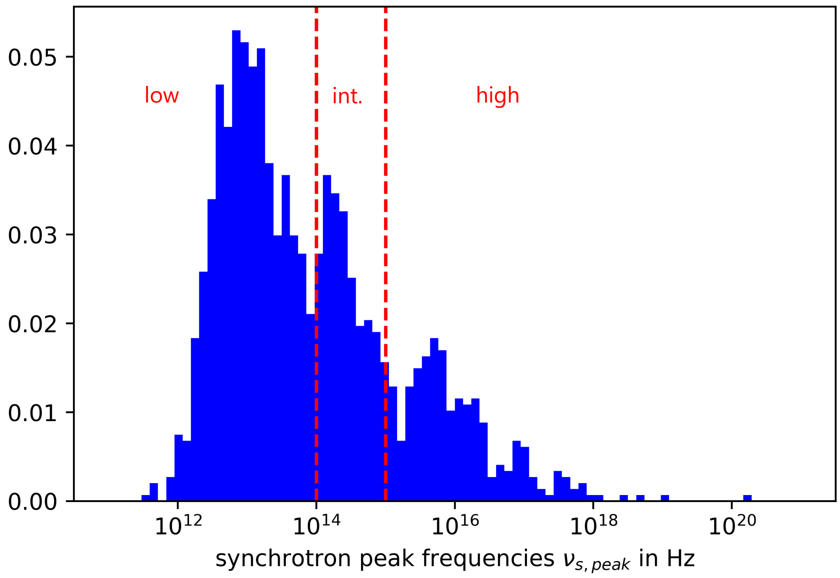

Figure 5.2: The histogramm shows the normalized distribution of the synchrotron peak frequencies, if measured respectively. The values are given in the observer frame. For the 1916 used blazars in this work 1472 showed an actually measured value for this quantity. The dotted red lines separate the blazars into low-, intermediate- and high-peaked.

5.3 Performance of the 4LAC Stacking Analysis

Since the work of this thesis was about to give an estimation of the expected performance of the 4LAC-DR2 stacking analysis, it was to first generate Monte Carlo (MC) simulations as pseudo-experiments in IceCube each containing a possible data sample of neutrino events in the time span of 9 years on which the stacking analysis could be run [35]. In order to obtain the statistical behaviour of the IceCube pseudo-experiments assuming the null hypothesis H_0 corresponding to the truth, one simulation sample was generated by only considering neutrino events based on the defined background, i.e. the conventional atmospheric and the diffuse astrophysical flux. The neutrino events of these simulations were randomly drawn from the model describing the background. The energy spectrum for example was modelled by the power law dependencies $\sim E^{-\gamma}$ with $\gamma = 3.7$ for the conventional atmospheric and $\gamma = 2.28$ for the diffuse astrophysical component (see also 4.1).

Each trial of the generated MC samples corresponded to a possible outcome of an IceCube experiment for the case that there would indeed only be the background neutrino fluxes and blazars would not portray contributing point sources.

In total the background sample based on H_0 consisted of around 100 000 trials. For each trial a $\mathcal{TS}$ value could be calculated by running the stacking analysis it.

The obtained distribution of these $\mathcal{TS}$ values was used as a numerical PDF and built the basis to perform a hypothesis test on. The median of this distribution turned out to be 0. This corresponds to the fact of using the unbinned maximum likelihood method 4.1 within the stacking analysis. Since the likelihood function $\mathcal{L}(n_s, \gamma|x)$ which gives the probability for the signal hypothesis H_1 to be true is maximized with respect to the spectral index γ and especially here the expected number of astrophysical neutrino events n_s, the best fit is found in $n_s = 0$ for assuming the null hypothesis and only background events. Thus the $\mathcal{TS}$ value in 4.10 is indeed 0 for the very most of the pseudo-experiments.

Nevertheless there is still a probability to obtain higher $\mathcal{TS}$ values under a valid null hypothesis and indeed only background events. Further the critical value, i.e. the lower threshold for $\mathcal{TS}$ values which have a p-value smaller than $3\sigma = 0.00135$ (see 4.2) could be determined to 8.49. The critical value is crucial for the case of discovery potential as it defines the region of rejecting the null hypothesis. For the discovery potential the $\mathcal{TS}$ values are larger than the critical value in 50% of the cases. Analogous for the case of sensitivity flux the $\mathcal{TS}$ values are larger than the median in 90% of the cases for the pseudo-experiments. The distribution of the $\mathcal{TS}$ values obtained under assuming the null hypothesis is shown in figure 5.3.

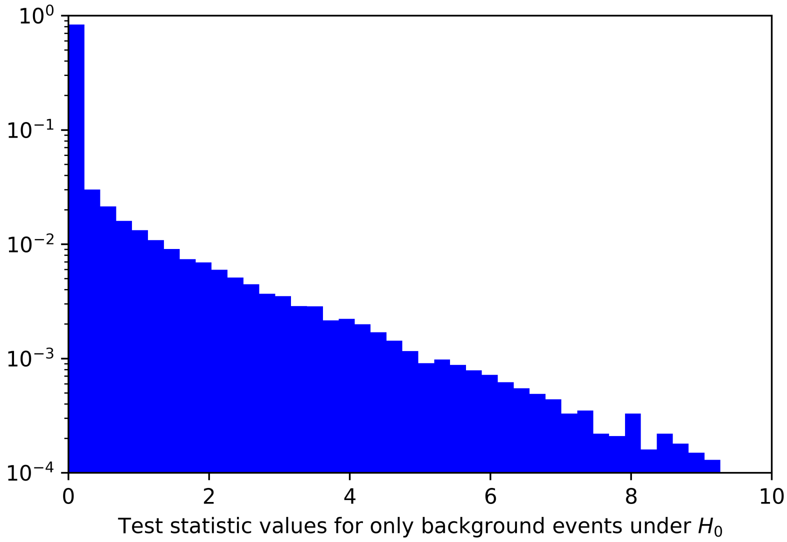

Figure 5.3: The histogramm shows the distribution of $\mathcal{TS}$ values obtained for assuming that the null hypothesis is true.

Furthermore another sample of simulations had to be generated under the assumption of a correct signal hypothesis H_1, in which blazars actually portray point sources for astrophysical neutrinos. Additional to events from the defined background, here neutrinos were injected according to the signal model, i.e. they were drawn from the point sources. As already stated the spatial distribution was obtained numerically (see 4.1) and the spectral energy dependence was again based on a power law:

$$\frac{d\Phi}{dE} = \Phi_0 \cdot (E/E_0)^{-\gamma} \tag{5.2}$$

with $\gamma = 2.0$. In total 80 000 signal trials were run, each corresponding to a concrete possible outcome of an experiment in IceCube assuming that the signal hypothesis H_1 is true. Apart from generating both of the MC samples we actually made use of the possibility to assign relative weights W^k to the sources for the stacking analysis and therefore the calculation of the $\mathcal{TS}$ values as it was stated in 5.1. For the 1916 used sources which are located in the Northern Hemisphere as defined before, the ones that are closer than 0.5° in angular distance to each other were treated separately. The reason behind this step is the limited resolution of IceCube for the angular reconstruction, i.e. the uncertainty of the arrival direction, which was introduced as σ_i in the context of the dataset in 4.1.
The histogram 5.4 shows the distribution of the estimated angular uncertainty for

(simulated) Monte Carlo events for both, the conventional atmospheric and the diffuse astrophysical flux.

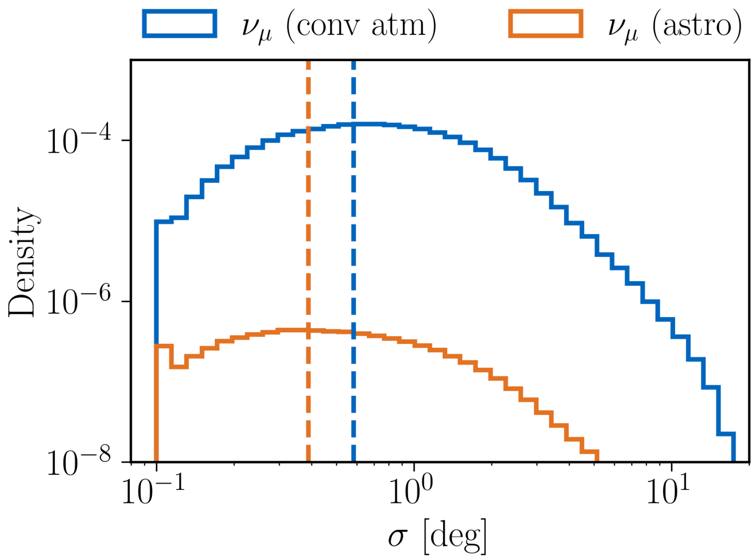

Figure 5.4: Histogram of the estimated angular uncertainty of Monte Carlo events for atmospheric and diffuse astrophysical fluxes. The dotted lines represent the respective median values of the distributions.
This histogram was made and provided by Chiara Bellenghi.

The fixed numerical value of 0.5° is based on the median of the uncertainty distributions in 5.4 respectively and was chosen to have a reasonable threshold over the whole detection area, since the resolution strongly depends on the declination. This information was then further used to apply the individual weights W^k to the signal PDFs, in the sense it was defined in equation 5.1 for the stacking method. Specifically for each source, where there was found another one within the set limit, a relative weight of 1/2 and for the rest just a relative factor of 1 was applied. The idea here was that for weighting the sources being 'too close' in the here defined sense one gets rid of the fact that one was actually double counting a single neutrino event. Applying these weights lead to the scenario that in the end there was a higher flux of blazar neutrinos necessary to be seen over the background, since the probability that the signal hypothesis H_1 is valid under the condition of the received dataset is slightly reduced compared to the case of equally weighting all the sources. Finally mind that the weights had to be normalized, so that it holds $\sum_{k=1}^{M} W^k = 1$.

It appears that the blazars located within 0.5° to another only come up in pairs. An illustration of the general situation is given by 5.5.

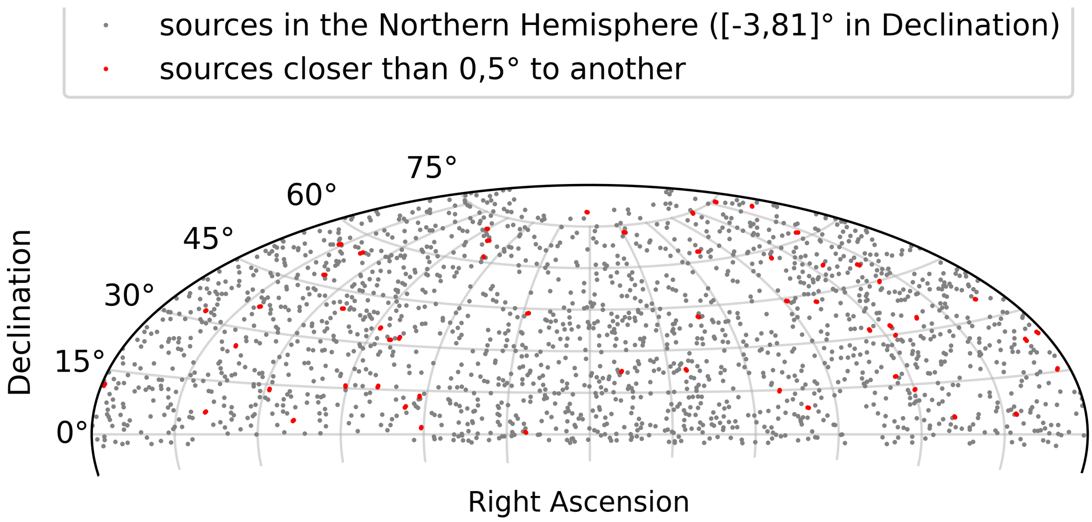

Figure 5.5: The skymap shows all 1916 considered blazars, where the ones that have a partner within an angular distance of 0.5° are marked red.

As the work was about to give an estimation of the performance of the stacking analysis, the obtained $\mathcal{TS}$ values had to be treated furtherly. For each of the pseudo-experiments, i.e. 100 000 trials which were generated under the assumption that the null hypothesis is correct and 80 000 trials which were generated under the assumption that the signal hypothesis states the truth, a certain number of neutrinos which were emitted by the considered blazars and actually detected in the pseudo-experiment was inserted. Each of these numbers was drawn randomly from poisson distributions for which the mean values were handed over for each of the pseudo-experiments. For generating the trial sample under the assumption that the null hypothesis is valid these mean values were apparently set to 0 as there should not be any neutrinos emitted by blazars. For the sample based on the assumption that the signal hypothesis is true, 16 different values for these mean numbers were used, covering a range of $40 - 70$ in steps of 2. 5000 trials were run for each of these values leading to the total amount of 80 000 pseudo-experiments assuming the signal hypothesis is true.
Assuming the realization of a certain expected number N_μ of neutrinos that were first emitted by blazars and then actually observed in IceCube within the pseudo-experiments, not all values for the number of actual detected neutrino events would be realized equally likely. Since the detection of these neutrinos can be modelled as a counting experiment the probability of actually detecting a certain number of these neutrinos is given by a poisson distribution 5.3 using the expected number N_μ as the mean value.
Thus the obtained distribution of $\mathcal{TS}$ values had to be re-weighted, in the sense of how likely the number of actual detected blazar neutrinos and therefore the outcome of the pseudo-experiment would be under the assumption of a certain expected number of detected blazar neutrinos. Each of the $\mathcal{TS}$ values could be associated to a specific number k of detected neutrino events caused by the flux from blazars. They were gathered in groups which showed the same associated number k to re-weight them.
At first the groups were normalized respectively. Assuming the realization of a certain expected number N_μ of detected neutrinos coming from the considered blazars, the corresponding poisson weights

$$P_{N_\mu}(k) = \frac{N_\mu^k}{k!} e^{-N_\mu} \tag{5.3}$$

could be applied to the contribution of each $\mathcal{TS}$ group which showed the same number k. The expected number of detected neutrinos for the pseudo-experiments which was used as the mean number N_μ in the poisson distribution was iterated through several numerical values to see for which of the values the conditions for sensitivity and discovery potential would be fulfilled respectively. That is, for the case of discovery potential we determined the necessary mean number N_μ so that in 50% of the pseudo-

experiments a $\mathcal{TS}$ value with a p-value smaller than $3\sigma = 0.00135$ was obtained. Analogous for the case of sensitivity the determined mean number lead to $\mathcal{TS}$ values with a p-value smaller than 0.5 in 90% of the pseudo-experiments.
The results for this are listed in the following table 5.1.

	mean number N_μ
sensitivity	46.16
discovery potential	67.91

Table 5.1: This table shows the results of the sensitivity study by means of which mean number of detected neutrino events would be necessary for sensitivity and discovery potential.

Eventually to put this into further context it should be mentioned that these mean numbers have to be seen as the necessary expected numbers of detected neutrinos emitted by the considered blazars over the regarded time span of 9 years which the work is based on.
The final $\mathcal{TS}$ distribution for the assumption of only background events as well as the weighted distributions for the assumption of a valid signal hypothesis H_1 in which blazars indeed portray neutrino point sources are shown in 5.6. The cases for sensitivity and discovery potential are plotted respectively.

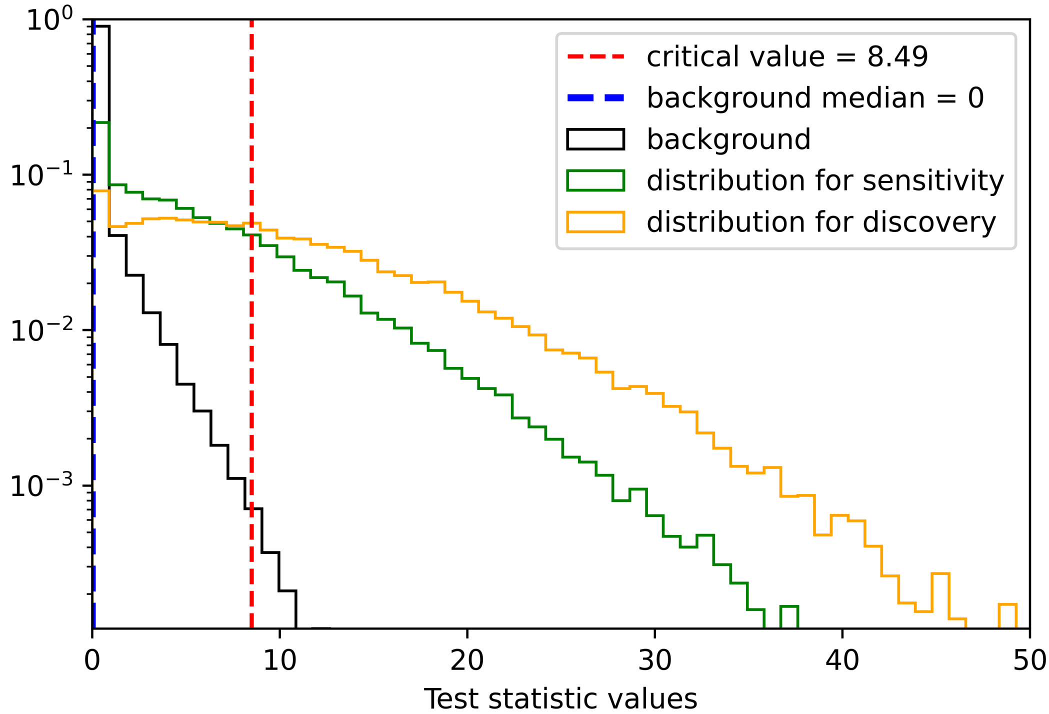

Figure 5.6: The plot shows the distribution of $\mathcal{TS}$ values for the case of a valid null hypothesis from which the median and critical value were calculated. Further the distribution of the $\mathcal{TS}$ values are plotted respectively in the case of the determined sensitivity and discovery potential flux

Finally the determined mean numbers N_μ which represent the number of expected neutrino detections due to a finite emission strength of blazars may be translated into an actual total flux of neutrinos coming from all considered blazars together. Given a certain flux Φ of neutrinos emitted by the blazars considered in this work the expected number N_μ of detected (muon) neutrino [2] events per unit time in IceCube can be calculated by:

$$\frac{dN_\mu}{dt} = \frac{1}{\Delta\Omega_{hem}} \int dE \int d\Omega \; A_{eff}(E, \Omega) \frac{d\Phi}{dE} \tag{5.4}$$

A_{eff} is the effective area and includes statistical properties like the cross section for neutrinos to interact in IceCube. Thus this quantity represents the detection probability. The normalization by the solid angle of the considered region, i.e. declination $\delta \in [-3, 81]^\circ$, is needed here since the differential flux is modelled by a power law

$$\frac{d\Phi}{dE} = \Phi_0 \left(\frac{E}{E_0}\right)^{-\gamma} \tag{5.5}$$

which is integrated of the solid angle as it is the total flux of all blazars together.
Further the results in table 5.1 are values for the expected number of events over a time span of ($\Delta t =$) 9 years, therefore the equation reduces to:

$$N_{mu} = \Phi_0 \frac{1}{\Delta\Omega_{hem}} \Delta t \int dE \int d\Omega \; A_{eff}(E, \Omega) \frac{d\Phi}{dE} \tag{5.6}$$

To finally come up with a flux Φ_0 based on the calculated number N_μ of expected events the integral had to be solved numerically using the spectral index $\gamma = 2.0$. The dependence of the effective area on the solid angle and the neutrino energy could be obtained numerically via MC simulations.
The results for the flux constant Φ_0 based on the determined expected neutrino events given in table 5.1 are listed in the following table 5.2.

	Φ_0 in $(\text{GeVcm}^2\text{s})^{-1}$
sensitivity	$3.43 \cdot 10^{-15}$
discovery potential	$5.05 \cdot 10^{-15}$

Table 5.2: The table lists the results for the necessary sensitivity and discovery potential flux respectively.

The results for Φ_0 may be used to calculate the differential flux modelled by a power law as stated in equation 5.5 with the normalization of the energy set $E_0 = 1$ TeV.

[2] We calculated the expected numbers of detected events and fluxes only for muon neutrinos as the work is only based un op-going muon tracks over 9 years in IceCube.

Finally it should be mentioned that since the work is based on only muon tracks detected over 9 years in IceCube the number N_μ and the fluxes Φ only consider muon neutrinos. The total flux of neutrinos coming from blazars is expected to be three times of the here calculated one as one expects equal parts of neutrino flavors due to ν oscillations.

The obtained results shown above already refer to an improved stacking analysis as we made use of the relative weights W^k to apply them to the several possible sources. To further evaluate the impact of applying these weights based on the angular resolution of IceCube and finally on the angular separation of the blazars the results could be compared to the case of equally weighting them. The results for the latter are listed in table 5.3 below.

	mean number N_μ	Φ_0 in $(\mathrm{GeVcm}^2\mathrm{s})^{-1}$
sensitivity	45.99	$3.42 \cdot 10^{-15}$
discovery potential	67.78	$5.04 \cdot 10^{-15}$

Table 5.3: This table lists the results for the case of equally weighting all sources.

The values N_μ and Φ_0 should be used in the same context as above. The results were pretty close to the ones which were obtained applying individual weights, so the impact here is actually not that big. In explicit numbers the necessary fluxes for sensitivity and discovery potential in the case of applying equal weights showed a difference of only $0.2 - 0.3$ % compared to the fluxes from the improved analysis in table 5.2.

6 Conclusion and Outlook

Since IceCube is detecting a diffuse flux of astrophysical neutrinos additional to an atmospheric background, one of the questions arising is about the origin of the astrophysical events. Promising candidates for possible sources are found in blazars. An experimental justification to consider blazars as neutrino sources was found in the course of the observations about the blazar TXS $0506+056$ which showed significant evidence that it indeed emits a flux of astrophysical neutrinos. The work in this thesis was based on pseudo-experiments testing blazars which were provided by the 4LAC-DR2 catalog as point sources for neutrino emission. In summary we determined the neutrino fluxes which have to be necessarily emitted by the considered blazars located in the Northern Hemisphere so that IceCube would actually observe them over the background flux consisting of the conventional atmospheric and a diffuse astrophysical component. For the case of an ideed realized sensitivity flux $\Phi_0 = 3.43 \cdot 10^{-15}$ $(\mathrm{GeVcm^2s})^{-1}$ IceCube would deliver a $\mathcal{TS}$ value with a p-value smaller than 0.5 in 90% of the cases of conducted experiments. For a flux emitted of the strength $\Phi_0 = 5.05 \cdot 10^{-15}$ $(\mathrm{GeVcm^2s})^{-1}$ for discovery potential IceCube would deliver a $\mathcal{TS}$ value with a p-value smaller than 0.00135 in 50% of the cases of conducted experiments and therefore one would reject the null hypothesis on a 3σ confidence in disfavour of the signal hypothesis which assumes blazars to be neutrino point sources. In other words: The work of the thesis respectivley sets an upper limit for the astropyhsical neutrino flux Φ which is produced by the considered blazars in case IceCube would actually not be able to observe the flux with statistical significance over the background [1]. The potential outcomes of the experiments are based on only up-going muon tracks over the considered time span of 9 years and were generated as pseudo-experiments within this work. The final results of Φ_0 have to be used in the context of the power law model for the differential flux :

$$\frac{d\Phi}{dE} = \Phi_0 \left(\frac{E}{E_0}\right)^{-\gamma} \tag{6.1}$$

This should be seen as a total flux of muon neutrinos emitted by all the considered blazars located in the Northern Hemisphere. In this thesis it was assumed that the considered blazars all show the same strength in their emission of neutrinos. Further

[1] The confidence levels for this statement can be obtained by the definition of sensitivity and discovery potential.

the limited angular resolution of IceCube was respected. The re-weighting of sources that lie within an angular distance of 0.5° of another one lead to an increased necessary flux but had not shown crucial impact. Actually one could think of further classifications of the considered blazars for which different relative weights could improve the stacking analysis. An example could directly be the observation and classification into different variable emission strengths of the point source candidates weighting them in correspondence to their relative contribution to the total flux Φ. For instance a correlation between the the electromagnetic and neutrino emission strength could not be observed, but other models respecting different properties like the characteristic synchrotron peak frequency $\nu_{s,peak}$ or the redshift of the sources might be able to help out to improve the stacking analysis in the future.

7 Appendix

The following part should give a justification of the application of poisson weights as the probability to detect an actual number k of neutrino events given a certain expected number N_μ.
For a given differential neutrino flux $d\Phi/dE$ the expected number N_μ of detected neutrino events in IceCube out of this flux can be calculated by the relation

$$N_{mu} = \Phi_0 \frac{1}{\Delta\Omega_{hem}} \Delta t \int dE \int d\Omega \; A_{eff}(E, \Omega) \frac{d\Phi}{dE} \tag{7.1}$$

That is, the effective area corresponds to the probability, depending on the energy and the solid angle, that a neutrino belonging to the flux is actually detected in IceCube, i.e. it can be seen analogously to a cross section.
Further an effective probability P can be derived from this. P is the effective probability that an arriving neutrino of this flux might actually interact and be detected in an event in IceCube. Since the time integrated flux, i.e. $\Phi_0 \cdot \Delta t$, might directly be translated to a certain number of arriving neutrinos n it holds that the probability P can be described by

$$N_\mu = P \cdot n \tag{7.2}$$

As stated, the quantity P expresses an effective probability integrated over the whole considered range of energy and the considered solid angle. It is in fact the probability for an arriving neutrino at IceCube to be detected respecting the dependence on the energy and the solid angle of both, the effective area and the differential flux.
Therefore the detection might be modelled as a counting experiment, assuming statistical independence of the events. The assumption is apparently justified in the present case of independent neutrinos. The probability p_k to actually detect a number k for a certain probability P that a event is caused by a single neutrino arriving and a number n of total arriving neutrinos is then given by the binomial distribution:

$$p_k = P^k (1-P)^{n-k} \begin{pmatrix} n \\ k \end{pmatrix} \tag{7.3}$$

Assuming that the effective probability is small, i.e. $P \to 0$ (this is indeed justified since the cross section for neutrinos and finally the effective area is very small), and a large total number of arriving neutrinos, i.e. especially for $n \to \infty$, it holds that $(1-P)^{n-k} \approx 1$ and

$$\lim_{n\to\infty} \begin{pmatrix} n \\ k \end{pmatrix} = \lim_{n\to\infty} \frac{n!}{k!(n-k)!} = \frac{n^k}{k!} \tag{7.4}$$

Thus the probability p_k to detect k neutrinos out of the total n becomes:

$$\lim_{n\to\infty} p_k = \lim_{n\to\infty} \frac{(n \cdot P)^k}{k!} \left(1 - \frac{n \cdot P}{n}\right)^n = \frac{(n \cdot P)^k}{k!} e^{-n \cdot P} \tag{7.5}$$

Using the relation $N_\mu = n \cdot P$ from above this gets us to the final poisson distribution

$$p_k = \frac{N_\mu^k}{k!} e^{-N_\mu} \tag{7.6}$$

with N_μ as the expected number of detected events as we wished to derive [36].

List of Figures

2.1 Feynman diagram of deep inelastic scattering (DIS) for a muon (anti-) neutrino off a nucleus via the exchange of a $W^{\pm}$-boson (CC) where also a hadronic shower is produced. The outgoing muon can be detected as evidence. At each vertex here the conservation of momentum, charge and the leptonic flavor is respected [16]. 9
2.2 The figure shows the differential flux of the cosmic ray in an energy range form 1 - 10^{12} GeV. It turns out that it can be described by power law dependencies, $d\Phi/dE \propto E^{-\gamma_i}$, for several sub-regions i of the considered energy spectrum. [18] 10
2.3 The figure gives an illustration of the general situation for IceCube detecting atmospheric and astrophysical neutrino events [22] 12
2.4 The plot shows the dependence of the neutrino fluxes observed by IceCube on the neutrino energy, i.e. the conventional atmospheric background and the diffuse astrophysical component. The y-axis which shows the counting for events in one bin which is proportional to the differential flux and is therefore considered equivalent in this context. The blue curve shows the behaviour of atmospheric neutrinos whereas the red one shows the behaviour of the diffuse astrophysical neutrino flux. The two curves are obtained by best-fit parameters which model the differential fluxes respectively The black crosses are experimental data for the observed total flux.[23] 13

3.1 Illustration of the Cherenkov-effect. The figure shows the emitted cone of Cherenkov light, including the opening angle for the example of a muon-track [25]. 16
3.2 This figure is a visual representation of the different event topologies that might appear in IceCube caused by neutrinos of different flavors crossing the detector [30]. 18

3.3 Illustration of the detector of IceCube Neutrino Observatory. It consists of the IceCube Lab (laboratory on the ground), IceTop (an surface array on top) and the IceCube in-ice array, placed underground in the antarctic ice [23]. To compare the size of the detector the Eiffel tower is placed next to it to scale. 19

4.1 This sketch should give an illustration of the overall situation of a hypothesis test. The blue curve represents the $\mathcal{TS}$ PDF obtained under the assumption that the null hypothesis is valid. here in this work this is realized by assuming only background events. The red curve shows the $\mathcal{TS}$ PDF in the case that the defined signal hypothesis corresponds to the truth. The sketch shows the example for sensitivity where for 90% of the cases the $\mathcal{TS}$ values gained under the signal hypothesis are larger than the median of the PDF for a valid null hypothesis. The case of discovery potential is analogous. 25

5.1 Artistic illustration of the general situation assuming that blazars are actual sources of astrophysical neutrinos [34]. 30

5.2 The histogramm shows the normalized distribution of the synchrotron peak frequencies, if measured respectively. The values are given in the observer frame. For the 1916 used blazars in this work 1472 showed an actually measured value for this quantity. The dotted red lines separate the blazars into low-, intermediate- and high-peaked. 30

5.3 The histogramm shows the distribution of $\mathcal{TS}$ values obtained for assuming that the null hypothesis is true. 32

5.4 Histogram of the estimated angular uncertainty of Monte Carlo events for atmospheric and diffuse astrophysical fluxes. The dotted lines represent the respective median values of the distributions. This histogram was made and provided by Chiara Bellenghi. 33

5.5 The skymap shows all 1916 considered blazars, where the ones that have a partner within an angular distance of 0.5° are marked red. 34

5.6 The plot shows the distribution of $\mathcal{TS}$ values for the case of a valid null hypothesis from which the median and critical value were calculated. Further the distribution of the $\mathcal{TS}$ values are plotted respectively in the case of the determined sensitivity and discovery potential flux 37

List of Tables

5.1 This table shows the results of the sensitivity study by means of which mean number of detected neutrino events would be necessary for sensitivity and discovery potential. 36
5.2 The table lists the results for the necessary sensitivity and discovery potential flux respectively. 38
5.3 This table lists the results for the case of equally weighting all sources. . 39

Bibliography

[1] M. Ajello et al. "The Fourth Catalog of Active Galactic Nuclei Detected by the Fermi Large Area Telescope". In: *The Astrophysical Journal* 892.2 (Apr. 2020), p. 105. DOI: 10.3847/1538-4357/ab791e. URL: https://doi.org/10.3847/1538-4357/ab791e.

[2] B. Lott, D. Gasparrini, and S. Ciprini. *The Fourth Catalog of Active Galactic Nuclei Detected by the Fermi Large Area Telescope – Data Release 2*. 2020. DOI: 10.48550/ARXIV.2010.08406. URL: https://arxiv.org/abs/2010.08406.

[3] "Evidence for High-Energy Extraterrestrial Neutrinos at the IceCube Detector". In: *Science* 342.6161 (Nov. 2013). DOI: 10.1126/science.1242856. URL: https://doi.org/10.1126/science.1242856.

[4] M. A. et al. "Multimessenger observations of a flaring blazar coincident with high-energy neutrino IceCube-170922A". In: *Science* 361.6398 (July 2018). DOI: 10.1126/science.aat1378. URL: https://doi.org/10.1126/science.aat1378.

[5] M. A. et al. "Neutrino emission from the direction of the blazar TXS 0506056 prior to the IceCube-170922A alert". In: *Science* 361.6398 (July 2018), pp. 147–151. DOI: 10.1126/science.aat2890. URL: https://doi.org/10.1126/science.aat2890.

[6] W. Pauli. *'Dear radioactive ladies and gentlemen'*. Dec. 1930.

[7] C. L. Cowan et al. "Detection of the Free Neutrino: a Confirmation". In: *Science* 124.3212 (July 1956), pp. 103–104. DOI: 10.1126/science.124.3212.103. URL: https://doi.org/10.1126/science.124.3212.103.

[8] M. H. Ahn et al. "Measurement of neutrino oscillation by the K2K experiment". In: *Physical Review D* 74.7 (Oct. 2006). DOI: 10.1103/physrevd.74.072003. URL: https://doi.org/10.1103/physrevd.74.072003.

[9] Y. Fukuda et al. "Evidence for Oscillation of Atmospheric Neutrinos". In: *Physical Review Letters* 81.8 (Aug. 1998), pp. 1562–1567. DOI: 10.1103/physrevlett.81.1562. URL: https://doi.org/10.1103/physrevlett.81.1562.

[10] Z. Maki, M. Nakagawa, and S. Sakata. "Remarks on the Unified Model of Elementary Particles". In: *Progress of Theoretical Physics* 28.5 (Nov. 1962), pp. 870–880. DOI: 10.1143/ptp.28.870. URL: https://doi.org/10.1143/ptp.28.870.

[11] B. Pontecorvo. *Neutrino Experiments and the Problem of Conservation of Leptonic Charge*. 1967.

[12] J. Thomas and P. Vahle. *Neutrino Oscillations: Present Status And Future Plans*. World Scientific Publishing Company, 2008. ISBN: 9789814474092. URL: https://books.google.de/books?id=BlDICgAAQBAJ.

[13] D. G. Michael et al. "Observation of Muon Neutrino Disappearance with the MINOS Detectors in the NuMI Neutrino Beam". In: *Physical Review Letters* 97.19 (Nov. 2006). DOI: 10.1103/physrevlett.97.191801. URL: https://doi.org/10.1103/physrevlett.97.191801.

[14] K. Eguchi et al. "First Results from KamLAND: Evidence for Reactor Antineutrino Disappearance". In: *Physical Review Letters* 90.2 (Jan. 2003). DOI: 10.1103/physrevlett.90.021802. URL: https://doi.org/10.1103/physrevlett.90.021802.

[15] D. S. Parno and K. Valerius. "Probing the neutrino mass scale with the KATRIN experiment". In: *Europhysics News* 53.1 (2022), pp. 24–27. DOI: 10.1051/epn/2022107. URL: https://doi.org/10.1051/epn/2022107.

[16] J. A. Formaggio and G. P. Zeller. "From eV to EeV: Neutrino cross sections across energy scales". In: *Reviews of Modern Physics* 84.3 (Sept. 2012), pp. 1307–1341. DOI: 10.1103/revmodphys.84.1307. URL: https://doi.org/10.1103/revmodphys.84.1307.

[17] D. Perkins. *Particle Astrophysics, Second Edition*. Oxford Master Series in Physics. OUP Oxford, 2008. ISBN: 9780199545469. URL: https://books.google.de/books?id=BWExNAAACAAJ.

[18] M. J. Huber. "Sensitivity Studies for Blazar Stacking Searches with the IceCube Neutrino Observatory". MA thesis. Technische Universität München, 2015.

[19] K. Olive. "Review of Particle Physics". In: *Chinese Physics C* 38.9 (Aug. 2014), p. 090001. DOI: 10.1088/1674-1137/38/9/090001. URL: https://doi.org/10.1088/1674-1137/38/9/090001.

[20] J. K. Becker. "High-energy neutrinos in the context of multimessenger astrophysics". In: *Physics Reports* 458.4-5 (Mar. 2008), pp. 173–246. DOI: 10.1016/j.physrep.2007.10.006. URL: https://doi.org/10.1016/j.physrep.2007.10.006.

[21] A. R. Bell. "The acceleration of cosmic rays in shock fronts - I". In: *Monthly Notices of the Royal Astronomical Society* 182.2 (Feb. 1978), pp. 147–156. DOI: 10.1093/mnras/182.2.147. URL: https://doi.org/10.1093/mnras/182.2.147.

[22] URL: https://www.facebook.com/icecube.neutrino/photos/dozens-of-astrophysical-neutrinos-100-thousand-atmospheric-neutrinos-and-100-bil/10156104336976867/.

[23] M. G. Aartsen et al. "OBSERVATION AND CHARACTERIZATION OF A COSMIC MUON NEUTRINO FLUX FROM THE NORTHERN HEMISPHERE USING SIX YEARS OF ICECUBE DATA". In: *The Astrophysical Journal* 833.1 (Dec. 2016), p. 3. DOI: 10.3847/0004-637x/833/1/3. URL: https://doi.org/10.3847/0004-637x/833/1/3.

[24] M. Aartsen et al. "The IceCube Neutrino Observatory: instrumentation and online systems". In: *Journal of Instrumentation* 12.03 (Mar. 2017), P03012–P03012. DOI: 10.1088/1748-0221/12/03/p03012. URL: https://doi.org/10.1088/1748-0221/12/03/p03012.

[25] K. M. Krings. "Search for Galactic and Extra-Galactic Neutrino Emission with IceCube". MA thesis. Technische Universität München, 2018.

[26] P. D. Group. *Particle Physics Booklet*. 2012.

[27] R. Abbasi et al. "An improved method for measuring muon energy using the truncated mean of dE/dx". In: *Nuclear Instruments and Methods in Physics Research Section A: Accelerators, Spectrometers, Detectors and Associated Equipment* 703 (Mar. 2013), pp. 190–198. DOI: 10.1016/j.nima.2012.11.081. URL: https://doi.org/10.1016/j.nima.2012.11.081.

[28] C. Bellenghi et al. *A New Search for Neutrino Point Sources with IceCube*. 2021. DOI: 10.48550/ARXIV.2107.08700. URL: https://arxiv.org/abs/2107.08700.

[29] T. K. Gaisser and M. Honda. "FLUX OF ATMOSPHERIC NEUTRINOS". In: *Annual Review of Nuclear and Particle Science* 52.1 (Dec. 2002), pp. 153–199. DOI: 10.1146/annurev.nucl.52.050102.090645. URL: https://doi.org/10.1146/annurev.nucl.52.050102.090645.

[30] M. Wallraff. "Design, Implementation and Test of a New Feature Extractor for the IceCube Neutrino Observatory". MA thesis. RWTH Aachen, 2010.

[31] J. Braun et al. "Methods for point source analysis in high energy neutrino telescopes". In: *Astroparticle Physics* 29.4 (May 2008), pp. 299–305. DOI: 10.1016/j.astropartphys.2008.02.007. URL: https://doi.org/10.1016/j.astropartphys.2008.02.007.

[32] J. Stettner. *Measurement of the Diffuse Astrophysical Muon-Neutrino Spectrum with Ten Years of IceCube Data*. 2019. DOI: 10.48550/ARXIV.1908.09551. URL: https://arxiv.org/abs/1908.09551.

[33] K. Schatto. "Stacked searches for high-energy neutrinos from blazars with IceCube". PhD thesis. Johannes Gutenberg-Universität Mainz, June 2014.

[34] URL: https://www.km3net.org/tag/detection-of-neutrinos-from-blazar/.

[35] T. Kontrimas et al. "The SkyLLH framework for IceCube point-source search". In: *Proceedings of 37th International Cosmic Ray Conference — PoS(ICRC2021)*. Sissa Medialab, July 2021. DOI: 10.22323/1.395.1073. URL: https://doi.org/10.22323/1.395.1073.

[36] A. J. Larkoski. *Elementary Particle Physics*. Cambridge University Press, May 2019. DOI: 10.1017/9781108633758. URL: https://doi.org/10.1017/9781108633758.